# Coupled MRT Lattice Boltzmann Study of Electrokinetic Mixing of Power-Law Fluids in Microchannels with Heterogeneous Surface Potential

Xuguang Yang[1,2], Lei Wang[3,*] and Baochang Shi[4]

[1] *School of Mathematics and Computational Science, Hunan First Normal University, Changsha 410205, Hunan, China*
[2] *Department of Applied Mathematics, The Hong Kong Polytechnic University, Hung Hom, Hong Kong*
[3] *School of Mathematics and Physics, China University of Geosciences, Wuhan, 430074, Hubei, China*
[4] *School of Mathematics and Statistics, Huazhong University of Science and Technology, Wuhan 430074, Hubei, China*

**Abstract.** The electrokinetic mixing, as a powerful technique in microfluidic devices, is widely used in many applications. In this study, a more general dynamic model, which consists of Poisson equation, Nernst-Planck equation and Navier-Stokes equations, is used to describe the electrokinetic mixing of non-Newtonian fluids in microchannels. Furthermore, a coupled multiple-relaxation-time (MRT) lattice Boltzmann (LB) framework is developed to solve this complicated multi-physics transport phenomenon. In numerical simulations, we mainly consider the effects of the arrangement of nonuniform surface potentials and the power-law index on the mixing efficiency and the volumetric flow rate. Numerical results show that the mixing efficiency and the volumetric flow rate of shear-thinning fluids are higher than that of shear-thickening fluids under the same condition. It is also shown that for both types of fluids, there should be a balance between the mixing and liquid transport in electrokinetic microfluidics.

## 1 Introduction

The micro-electro-mechanical systems (MEMS) have attracted more and more attentions in recent years due to its wide applications in biomedical, chemical analyses, drug de-

---

*Corresponding author.
*Email:* wangleir1989@126.com (L. Wang)

livery and so on [1–3]. In many practical microfluidic applications, the rheological behavior of the fluids must be considered since the used fluids have the non-Newtonian characteristics. Specifically, non-Newtonian effects are characterized by proper constitutive models which relate the dynamic viscosity and the rate of shear. Power-law fluid model is certainly the most popular because it is simple and able to fit a wide range of non-Newtonian fluids, such as solutions of blood, saliva, protein and DNA, polymeric solutions and colloidal suspensions. One important parameter in the power law fluid model is the fluid behavior index ($n$) which delineates the dependence of the dynamic viscosity on the rate of shear. If $n$ is smaller (greater) than one, the fluid demonstrates the shear-thinning (shear-thickening) effect that the viscosity of fluid decreases with the increase (decrease) of the rate of shear. If $n$ is equal to one, the fluids then exactly behave as Newtonian fluids. In this study, for the shear-thinning fluids, we consider the supramolecular polypeptide-DNA solutions as the working fluids, while for the shear-thickening fluids, the macromolecular protein solution is considered [4].

In such microfluidic devices, especially in the biomedical applications, rapid and homogenous mixing of two or more fluid species are required. Recently, electroosmotic flow (EOF), as an important non-mechanical actuating technique, has been widely utilized in fluid transport and mixing in microfluidic devices. The flow pattern of EOF in a microchannel is dependent on the surface charge distributions and the external applied electric fields. Existing research results show that the EOF in a microchannel with heterogeneous surface potential induces a vortex flow, which appears to be an excellent alternative to enhance mixing efficiency [5,6]. This mixing method has also received intensive attention because of the ease of control and integration with microfluidic devices. The EOF is a typical multiphysical transport phenomenon, which involves multiple processes including fluid flow, electrostatic interaction and species diffusion. Generally, this multiphysical transport problem can be described by the Poisson-Boltzmann (PB) model, which consists of the PB equation for the internal electrical potential and the Navier-Stokes equation for the flow field of electrolyte solutions. The PB equation is derived from the assumption that the ionic distribution in the electrical double layer (EDL) is to follow the equilibrium Boltzmann distribution [7,8]. However, the Boltzmann distribution is only applicable for the cases that the ionic distributions are not affected by the flows of the electrolyte solution or the bulk solution is far away from the charged surface. Thus, a more general model, could also be called Nernst-Planck (N-P) model, which utilizes the N-P equation for ions transport instead of Boltzmann distribution should be adopted in the study of EOF in microchannels with heterogeneous surface potential [9–12]. In the N-P model, the velocity of the flow field, the electrostatic potential and the ionic concentration are coupled together with strong nonlinearity, which poses great challenge to the numerical solution. In the past few years, the lattice Boltzmann method (LBM), which originates from lattice gas automata (LGA) and also could be derived from the kinetic Boltzmann equation, has emerged as an alternative powerful numerical method for simulating complex flows [13–15] and also has been extended to solve convection-diffusion-type equations [16–19]. In contrast to the classical PDE solvers, such as the

finite-difference method (FDM), the finite element method (FEM) and the finite volume method (FVM), the LBM is developed based on microscopic models and mesoscopic kinetic equations. This clear kinetic nature of LBM makes it quite easy to code; Particularly, the collision process involves only local computations and the streaming process can be realized by simple index shift operations, which makes LBM well suited for massive parallel computers [20]. Due to these advantages, the LBM has been successfully applied to simulate electrokinetic flows based on N-P model [12, 21, 22]. However, most existing works are focus on the behavior of Newtonian fluid. Due to the importance of bio-MEMS, many researchers have recently paid more attentions on the non-Newtonian fluid behavior of biofluids in electrokinetically driven flows. In the work by Hadigol et al. [23], the electroosmotic micromixing of non-Newtonian fluids with power-law property was numerically studied. The micromixing is realized by the EOF in microchannels with non-uniform surface potential. Zhao et al. presented an analysis of EOF of power-law fluids in a slit microchannel. The electroosmotic flow of power-law fluids in annulus and wavy microchannels was numerically studied by Shamshiri et al. [25] and Cho et al. [26], respectively. However, most of these analysis and numerical studies are based on the PB model. As we mentioned above, the Nernst-Planck model is more accurate than the PB model in the study of EOF in irregular microchannels or with heterogeneous surface potential.

In this work, we consider the micromixing of non-Newtonian fluid through using the electrokinetic driven flow with heterogeneous surface potential. The mathematical model consists of a Poisson equation for the distribution of EDL potential, the N-P equation for the distribution of charge density and the modified Navier-Stokes equations for the electrolyte solution flow. Based on this multi-physical dynamic model, a coupled multiple-relaxation-time (MRT) LBM is proposed to investigate the micromixing of non-Newtonian fluids with power-law behavior in microchannels. The rest of this paper is organized as follows. In Section 2, the problem statement and mathematical models of this study is introduced. In what follows, the coupled MRT-LBM framework is developed in Section 3. In Section 4, the numerical results and discussions are presented. Finally, some conclusions are given in Section 5.

## 2   Problem statement and mathematical models

In this study, we consider the EOF of power-law fluid in a rectangular microchannel with heterogeneous surface potential. The flow is assumed to be incompressible and fully developed. Fig. 1 illustrates the configuration of the computation domain where the surface heterogeneity is created by the microelectrodes which are embedded inside the solid near the solid-liquid interface [27]. The patterned surfaces with symmetric and asymmetric stepwise variation of surface potential are mainly studied in this work. As shown in Fig. 2(a), the patterned surface is heterogeneous with symmetrically distributed patches of length $L_n$ and $L_p$ on the lower and upper channels walls, whereas Fig. 2(b)
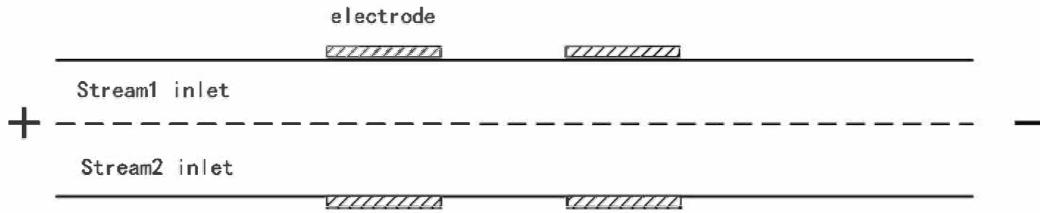
Figure 1: Schematic diagram of electroosmotic driven flow in microchannel with heterogeneous surface potential.
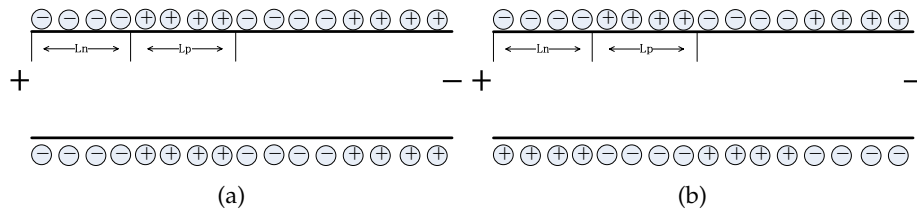


Figure 2: Schematic of the patterned surfaces with (a) symmetric and (b) asymmetric arrangement of patches.

represents a heterogeneous case where the patches on the lower and upper walls are asymmetric. In addition, the surface potentials with negative and positive charge are denoted by $\psi_n$ and $\psi_p$, respectively.

## 2.1 Electrokinetic model

Electrokinetic phenomenon is based on the existence of EDL, which is formulated by the interaction between the electrolyte solution and the solid surface. According to the theory of EDL, the induced electric potential $\psi$ is governed by the Poisson equation

$$\nabla^2\psi = -\frac{\rho_e}{\varepsilon_0\varepsilon_r},\tag{2.1}$$

where $\rho_e = \sum_i ez_kn_k$ is the net charge density, $e$ is the elementary charge, $z_k$ is the valence of the $k$ th ion, $n_k$ is the $k$ th ionic number concentration of the electrolyte solution, $\varepsilon_r$ is the dielectric constant of the solution and $\varepsilon_o$ is the permittivity of vacuum.

Generally, the ionic distribution in the EDL is usually assumed to follow the equilibrium Boltzmann distribution. However, the ionic distribution should be described by the N-P model when considering the heterogeneous surface potential. In the N-P model, the distribution of the ions in the solutions should be described as follows,

$$\frac{\partial n_k}{\partial t} + \nabla \cdot j_k = 0,\tag{2.2a}$$

$$j_k = n_k\mathbf{u} - D_k\nabla n_k - \frac{z_keD_k}{k_bT}n_k\nabla\psi,\tag{2.2b}$$

where $j_k$ is the flux density of the ion species $k$, $D_k$ is the diffusion coefficient, $k_B$ is the Boltzmann constant and $T$ is the absolute temperature. Under the assumptions that the system is in thermodynamic equilibrium and the ionic distributions are not affected by fluid flows, the N-P equation can be simplified by the Boltzmann distribution as,

$$n_k = n_0 \exp\left(-\frac{z_k e}{k_B T}\psi\right), \tag{2.3}$$

where $n_0$ is the ionic number concentration in the bulk solution.

Through introducing the following dimensionless variables,

$$\bar{\mathbf{x}} = \mathbf{x}/L, \qquad\qquad \bar{t} = t/t^*, \qquad\qquad \bar{\mathbf{u}} = \mathbf{u}/U^*, \tag{2.4a}$$

$$p' = pL/(\eta U^*), \qquad \bar{E} = E/E^*, \qquad \rho_e' = \rho_e L/(E^*\epsilon), \tag{2.4b}$$

$$St = L/t^* U^*, \qquad Pe = U^* L/D_k. \tag{2.4c}$$

These quantities are nondimensionalized using $L$, $U^*$, $t^*$, $E^*$, $\epsilon$ and $\eta$, which are a microchannel hydraulic diameter, a characteristic electroosmotic flow velocity, a characteristic time scale (e.g., for an applied forcing function), a characteristic electric field, an electrical permittivity of the medium and a dynamic viscosity, respectively. The N-P equation can be non-dimensionalized as

$$St Pe \frac{\partial \bar{n}_k}{\partial \bar{t}} + Pe \bar{\mathbf{u}} \cdot \nabla \bar{n}_k = \frac{LE^* z_k}{k_b T} \nabla \cdot (\bar{n}_k \nabla \bar{\psi}) + \nabla^2 \bar{n}_k, \tag{2.5}$$

where $\bar{\psi}$ is the electric potential nondimensionalized by $E^* d$.

## 2.2 The model of the power-law fluid flows

The flow of the electrolyte solution with power-law property can be described by the following mass and momentum equations [28],

$$\frac{\partial \rho \mathbf{u}}{\partial t} + \nabla \cdot \rho \mathbf{u} = 0, \tag{2.6a}$$

$$\frac{\partial \rho \mathbf{u}}{\partial t} + \nabla \cdot \rho \mathbf{u}\mathbf{u} = -\nabla P + \nabla \cdot \tau + \rho_e \mathbf{E}, \tag{2.6b}$$

where $\rho$ is the density of solution, $\mathbf{u}$ is the velocity vector, $P$ is the pressure, $\mathbf{E} = -(\nabla \psi + \nabla \phi)$ is the strength of the total electric field, $\phi$ is the external applied electrical potential. $\tau$ represents the shear stress defined by $\tau = \mu \dot{\gamma}$, $\mu$ is the dynamic viscosity of the flow, $\dot{\gamma}$ is the strain rate tensor defined as

$$\dot{\gamma} = 2\mathbf{S} = \left[\nabla \mathbf{u} + (\nabla \mathbf{u})^T\right],$$

where $\mathbf{S}$ is the shear rate and the superscript $T$ denotes the transposition operator.

Although the above equations are similar with the standard Navier-Stokes equations for Newtonian fluid flows, the dynamics viscosity $\mu$ is a function of shear rate $\dot{\gamma}$ rather than a constant in Newtonian fluid flows. In the power-law model [30], as one of the most commonly used non-Newtonian model, is usually used for modeling the shear-thinning or shear-thickening behavior of non-Newtonian fluids. The shear stress in the power-law model is defined by [28]

$$\tau_{\alpha\beta} = \mu\left(|\dot{\gamma}|\right)\dot{\gamma}_{\alpha\beta} = \mu_0|\dot{\gamma}|^{n-1}\dot{\gamma}_{\alpha\beta}, \tag{2.7}$$

where $\mu_0$ is the flow consistency coefficient, $|\dot{\gamma}| = \sqrt{2\mathbf{S}:\mathbf{S}}$ and $n$ is the power-law index. In general, the power-law fluids always appear three different types of fluids with the variation of the value of $n$. The case $n < 1$ corresponds to a shear-thinning or pseudoplastic fluid, whereas $n > 1$ corresponds to a shear-thickening or dilatant fluid and $n = 1$ reduces to the Newtonian fluid.

## 2.3　Species transport equation

The electrokinetic transport of uncharged sample species is considered in the present simulation. Assuming that there is no chemical reaction or absorption of species on the wall and the electrophoretic effect is also neglected, the transport of the solute in EOFs can be described by the following convection-diffusion equation,

$$\frac{\partial C}{\partial t} + \nabla\cdot(\mathbf{u}C) = D_c\nabla^2 C, \tag{2.8}$$

where $C$ is the species concentration and $D_c$ is the diffusion coefficient.

To quantify the mixing efficiency of the present study, we first introduce the concentration standard deviation $\sigma$ at various cross sections of the microchannel,

$$\sigma(x) = \sqrt{\frac{1}{H}\int_H [C(x,y) - C_\infty]^2 dy}, \tag{2.9}$$

where $H$ is the channel height, $C_\infty$ is the species concentrations with completely mixed state. Then, the mixing efficiency parameter $\alpha$ can be defined as $\alpha = 1 - \sigma_{out}/\sigma_{in}$.

## 2.4　Boundary conditions

In simulating the EOF of the power-law fluid through the microchannels with heterogeneous surface potential, we assume a longitudinal spatial periodicity for the finite domain under consideration. A constant electric potential due to externally applied electric field is applied to the inlets and a reference electric potential is set at the outlet. As the flow is electro-osmotically driven, there is no applied pressure and gravitational body force. Thus, the flow boundary conditions at the inlet and outlet are set as $\partial\mathbf{u}/\partial x = 0$. On the upper and lower walls, the non-slip boundary condition is adopted for the velocity field and the ionic concentration boundary condition in [31] is used. At the liquid-solid

interface, the homogeneous surface potential is approximated to zeta-potential ($\zeta$), the heterogeneous surface is achieved by implementing non-uniform surface potential $\psi_p$.

At the channel inlet where the sample meets buffer, the sample is injected at the upper half of the channel while the buffer moves in at the lower half of channel. Therefore, the species concentration is unity across the upper half of the channel and zero across the lower half of the channel. In addition, there is no mass flux along the channel wall. Thus, the boundary conditions of the species concentration are specified in the following way.

Inlet and Outlet: $C=0.0$ at $x=0$, $0<y<H/2$; $C=1.0$ at $x=0$, $H/2\leq y<H$; $\partial C/\partial x=0$ at $x=L$.

Wall surface: $\partial C/\partial y=0$ at $y=0,H$.

# 3 Numerical methods

## 3.1 The MRT-LBM for power-law non-Newtonian fluid flows

In the present work, the LBM with MRT collision operator is adopted to simulate the power-law fluids since it is more accurate and stable in the study of incompressible non-Newtonian flows and the evolution equation of the MRT-LBM reads [32]

$$f_i(\mathbf{x}+\mathbf{c}_i\Delta t,t+\Delta t)=f_i(\mathbf{x},t)-(\mathbf{M}^{-1}\Lambda\mathbf{M})_{ij}[f_j(\mathbf{x},t)-f_j^{eq}(\mathbf{x},t))]$$
$$+\Delta t\Big[\mathbf{M}^{-1}\Big(\mathbf{I}-\frac{1}{2}\Lambda\Big)\mathbf{M}\Big]_{ij}\overline{F}_j, \tag{3.1}$$

where $f_i(\mathbf{x},t)$ is the distribution function of a particle moving with $\mathbf{c}_i$ at position $\mathbf{x}$ and time $t$, $f_i^{eq}(\mathbf{x},t)$ is the local equilibrium distribution function, to recover the incompressible N-S equations accurately, we choose the He-Luo incompressible model as follows [33],

$$f_i^{eq}=\omega_i\Big\{\rho+\rho_0\Big[\frac{\mathbf{c}_i\cdot\mathbf{u}}{c_s^2}+\frac{(\mathbf{c}_i\cdot\mathbf{u})^2}{2c_s^4}-\frac{\mathbf{u}^2}{2c_s^2}\Big]\Big\}, \tag{3.2}$$

where $\rho_0$ is the reference density and provided that the flow is incompressible, $\rho_0$ is assumed to be a constant, for example, $\rho_0=1.0$. The discrete velocity $\mathbf{c}_i$ in the D2Q9 (two-dimensional-nine-velocity) model is defined as

$$\mathbf{c}_i=\begin{cases} (0,0)c, & i=0, \\ (\cos[(i-1)\pi/2],\ \sin[(i-1)\pi/2])c, & i=1,2,3,4, \\ 2(\cos[(i-5)\pi/2+\pi/4],\ \sin[(i-5)\pi/2+\pi/4])c, & i=5,6,7,8, \end{cases} \tag{3.3}$$

where $c=\Delta x/\Delta t$ is the particle velocity, $\Delta x$ and $\Delta t$ are the lattice spacing and time step and $c_s=c/\sqrt{3}$. The weight coefficients $\omega_i$ in the local equilibrium function are $\omega_0=4/9$, $\omega_i=1/9$ ($i=1\sim4$), $\omega_i=1/36$ ($i=5\sim8$).

$\overline{F}_i(\mathbf{x},t)$ is the discrete forcing term accounting for the external force and it is given by [34]

$$\overline{F}_i(\mathbf{x},t) = \omega_i \left[ \frac{\mathbf{c}_i \cdot \mathbf{F}}{c_s^2} + \frac{(\mathbf{Fu}+\mathbf{uF}):(\mathbf{c}_i\mathbf{c}_i - c_s^2\mathbf{I})}{2c_s^4} \right] \tag{3.4}$$

with $\mathbf{F} = \rho_e\mathbf{E}$.

$\Lambda$ is a diagonal relaxation matrix $\Lambda = diag(s_0,\cdots,s_8)$, where $0 < s_i < 2$. We would like to point out that, if $s_i$ are equal to each other, the MRT model will reduce to the LBGK model. $\mathbf{M}$ is the transformation matrix, for the generally used $D2Q9$ model, $\mathbf{M}$ is defined as

$$\mathbf{M} = \begin{pmatrix} 1 & 1 & 1 & 1 & 1 & 1 & 1 & 1 & 1 \\ -4 & -1 & -1 & -1 & -1 & 2 & 2 & 2 & 2 \\ 4 & -2 & -2 & -2 & -2 & 1 & 1 & 1 & 1 \\ 0 & 1 & 0 & -1 & 0 & 1 & -1 & -1 & 1 \\ 0 & -2 & 0 & 2 & 0 & 1 & -1 & -1 & 1 \\ 0 & 0 & 1 & 0 & -1 & 1 & 1 & -1 & -1 \\ 0 & 0 & -2 & 0 & 2 & 1 & 1 & -1 & -1 \\ 0 & 1 & -1 & 1 & -1 & 0 & 0 & 0 & 0 \\ 0 & 0 & 0 & 0 & 0 & 1 & -1 & 1 & -1 \end{pmatrix},$$

which can be used to project $f_i$, $f_i^{eq}$ and $\overline{F}_i$ onto the moment space with $\mathbf{m}=\mathbf{Mf}$, $\mathbf{m}^{eq}=\mathbf{Mf^{eq}}$ and $\widehat{\mathbf{F}} = (\mathbf{I}-1/2\Lambda)\mathbf{M\overline{F}}$, where $\mathbf{f}=(f_0,\cdots,f_8)^T$, $\mathbf{f}^{eq}=(f_0^{eq},\cdots,f_8^{eq})^T$ and $\overline{\mathbf{F}}=(\overline{F}_0,\cdots,\overline{F}_8)^T$.

The macroscopic velocity and density of fluid flow can be obtained from

$$\mathbf{u} = \sum_i \mathbf{c}_i f_i + \frac{\Delta t}{2}\mathbf{F}, \tag{3.5a}$$

$$\rho = \sum_i f_i. \tag{3.5b}$$

Through the Chapman-Enskog analysis, the incompressible Navier-Stokes equations (i.e., Eqs. (2.6a) and (2.6b)) can be recovered with

$$\mu(|\dot\gamma|) = \rho_0 c_s^2 \left( \frac{1}{s_8} - \frac{1}{2} \right) \Delta t. \tag{3.6}$$

In what follows, we will present a brief discussion on how to derive the effective viscosity of the power-law fluid $\mu_{\alpha\beta}$ with present MRT model. According to Eq. (2.7), $\mu_{\alpha\beta}$ is determined by the strain rate tensor $\mathbf{S}$. In the MRT-LBM, $\mathbf{S}$ can be evaluated by the non-equilibrium parts of the moments in the moment space [28, 29],

$$\partial_x u_x + \partial_y u_y = -\frac{m_1 - m_1^{eq} - 3\Delta t\mathbf{u}\cdot\mathbf{F}}{2\tau_1\Delta t}, \tag{3.7a}$$

$$\partial_x u_x - \partial_y u_y = -\frac{3[m_7 - m_7^{eq} - \Delta t(u_x F_x - u_y F_y)]}{2\tau_7 \Delta t}, \tag{3.7b}$$

$$\partial_x u_y + \partial_y u_x = -\frac{3(m_8 - m_8^{eq}) - 3\Delta t \mathbf{u} \cdot \mathbf{F}/2}{\tau_8 \Delta t}. \tag{3.7c}$$

Then, substituting the above equation into Eq. (2.7), one can obtain the effective viscosity $\mu_{\alpha\beta}$. And simultaneously, the relaxation parameter $1/s_8$ is derived via Eq. (3.6), which is used to perform the collision step. It is noted that in the simulation of the non-Newtonian fluid flows, the effective viscosity and relaxation parameters are functions of space and time, which should be updated in each iteration step. In the following simulations, the relaxation time factors are set as $s_0 = s_3 = s_5 = 0$, $s_1 = 1.1$, $s_2 = 1.0$, $s_4 = s_6 = 1.2$ and $s_7 = s_8$. The value of $s_8$ can be calculated by Eq. (3.6).

## 3.2　LBM for the Poisson equation

The Poisson equation is a very powerful tool for modeling the behavior of electrostatic systems. There are many fast Poisson solvers such the fast Fourier transform (FFT), multigrid solvers and so on. However, in this study, our main purpose is not only to develop a coupled LBM framework to simulate the electrokinetic flows but also to maintain the intrinsically parallel characteristic of LBM. Thus, we use the LBM to solve the Poisson equation which has been proposed by Chai and Shi [39].

The evolution equation of the model with a two-dimensional square lattice can be written as

$$\psi_i(\mathbf{x} + \mathbf{c_i}\delta_t, t + \delta_t) - \psi_i(\mathbf{x}, t) = -\frac{1}{\tau_\psi}[\psi_i(\mathbf{x}, t) - \psi_i^{eq}(\mathbf{x}, t)] + \delta_t \overline{\omega}_i RD, \tag{3.8}$$

where $\tau_\psi$ is the dimensionless relaxation time, $R$ is the righthand side term of the Poisson equation, $D = 2c^2(1/2 - \tau_\psi)\delta_t/5$, the weight coefficient $\overline{\omega}_0 = 0$, $\overline{\omega}_i = 1/4$ ($i \neq 0$), $\psi_i^{eq}$ is the equilibrium distribution function and defined as

$$\psi_i^{eq}(\mathbf{x}, t) = \begin{cases} (\omega_0 - 1.0)\psi(\mathbf{x}, t), & i = 0, \\ \omega_i \psi(\mathbf{x}, t), & i = 1-4, \end{cases} \tag{3.9}$$

where $\omega_i = 1/5$ ($i = 0-4$). The electric potential is calculated by

$$\psi(\mathbf{x}, t) = \frac{\sum\limits_{i=1}^{4} \psi_i(\mathbf{x}, t)}{1 - \omega_0}. \tag{3.10}$$

## 3.3　The MRT-LBM for the electrokinetic equations

In this section, we will present a novel MRT-LB model to solve the N-P equation. For the reason that a linearized equilibrium distribution function can be used in this model

and also to enhance the computational efficiency, a two-dimensional five-velocity (D2Q5) lattice model is implemented. The evolution equation with MRT collision operator for the distribution function $g_i(\mathbf{x},t)$ reads

$$g_i(\mathbf{x}+\mathbf{c}_i\Delta t,t+\Delta t)=g_i(\mathbf{x},t)-\widetilde{\mathbf{M}}^{-1}\mathbf{Q}[\widetilde{m}_i(\mathbf{x},t)-\widetilde{m}_i^{eq}(\mathbf{x},t)]+\Delta t[G_i(\mathbf{x},t)-S_i(\mathbf{x},t)], \quad (3.11)$$

where the moments $\widetilde{m}_i(\mathbf{x},t)$ are related to the distribution functions $g_i(\mathbf{x},t)$ by $\widetilde{\mathbf{m}}=\widetilde{\mathbf{M}}\mathbf{g}$, $\widetilde{\mathbf{M}}$ is the transformation matrix, $\mathbf{Q}$ is a diagonal matrix and the equilibrium moments $[\widetilde{m}_i^{eq}|i=0,1\cdots4]$ are given by

$$\widetilde{\mathbf{m}}^{eq}=(\widetilde{m}_0^{eq},\widetilde{m}_1^{eq},\widetilde{m}_2^{eq},\widetilde{m}_3^{eq},\widetilde{m}_4^{eq})^T=(n_k,un_k,vn_k,an_k,0), \quad (3.12)$$

where $u$ and $v$ are the velocity components obtained from the flow fields and $a$ is a constant, which is bounded by $a\in(-4,1)$ [35]. In this study, $a$ is set to be $-2$ in the following simulations. Additionally, due to the effect of the forcing term of hydrodynamic equations, an unwanted term $\nabla\cdot n_k\mathbf{F}$ is appeared in the electrokinetic equation. To eliminate this unwanted term, just like the work in [36–38], a correction term $G_i(\mathbf{x},t)$ is added on the right-hand of Eq. (3.11), which is defined as

$$G_i(\mathbf{x},t)=\left[\widetilde{\mathbf{M}}^{-1}\left(\mathbf{I}-\frac{1}{2}\mathbf{Q}\right)\widetilde{\mathbf{M}}\right]_{ij}\frac{\omega_j\mathbf{c}_j\cdot n_k\mathbf{F}}{\tilde{c}_s^2}. \quad (3.13)$$

The source term distribution function $S_i(\mathbf{x},t)$ is to handle the cross diffusion term in N-P equation, which is given by

$$S_i=[\widetilde{\mathbf{M}}^{-1}\mathbf{Q}\widetilde{\mathbf{M}}]_{ij}\omega_j\mathbf{c}_j\cdot BKn_k\nabla\psi, \quad (3.14)$$

where $B$ is a parameter and $K=ez_k/k_bT$. It is worth mentioning that the gradient term $\nabla\psi$ can be calculated locally at each node by

$$\nabla\psi(\mathbf{x},t)=-\frac{1}{c_s^2\tau_\psi\Delta t}\sum_i\mathbf{c}_i(\psi_i(\mathbf{x},t)-\psi_i^{eq}(\mathbf{x},t)). \quad (3.15)$$

Note that the above formula is derived from the LBM for the Poisson equation and there is no finite difference approximation, thus the locality of the algorithm inherent to the original LBM is maintained.

The discrete velocities in the $D2Q5$ model are given as follows:

$$\mathbf{c}_i=\begin{cases} (0,0)c, & i=0, \\ (\cos[(i-1)\pi/2], \sin[(i-1)\pi/2])c, & i=1,2,3,4. \end{cases} \quad (3.16)$$

In this model, $\tilde{c}_s^2=2c^2/5$, $\omega_i=1/5$.

The transformation matrix $\widetilde{\mathbf{M}}$ is defined as

$$\widetilde{\mathbf{M}}=\begin{pmatrix} 1 & 1 & 1 & 1 & 1 \\ 0 & 1 & 0 & -1 & 0 \\ 0 & 0 & 1 & 0 & -1 \\ -4 & 1 & 1 & 1 & 1 \\ 0 & 1 & -1 & 1 & -1 \end{pmatrix}. \quad (3.17)$$

The diagonal relaxation matrix $\mathbf{Q}$ is given by

$$\mathbf{Q} = diag(1, \sigma_\kappa, \sigma_\kappa, \sigma_e, \sigma_v). \tag{3.18}$$

Without loss of generality, the relaxation parameters are chosen as: $\sigma_\kappa = 1/\tau_{n_k}$ and $\sigma_e = \sigma_v = 1.1$. Further, the $k$th ion concentration $n_k$ is calculated by $n_k = \sum_i g_i$. Through the Chapman-Enskog analysis, the N-P equation can be recovered with $D_k = \tilde{c}_s^2 \left( \tau_{n_k} - \frac{1}{2} \right) \Delta t$.

# 4   Results and discussion

In this section, the electrokinetic flows in homogeneously and heterogeneously charged microchannels are numerically studied by the coupled MRT-LBM. The effects of power-law index and non-uniform surface potential on the mixing efficiency and liquid transport in EOF microfluidics have been fully considered.

## 4.1   Numerical validations

Before the numerical study of electrokinetic mixing of power-law fluid in microchannel, a simple electroosmotic flow of power-law fluid in a homogeneously charged microchannel with a width $H$ of $1\mu$m is simulated with the purpose of validating the present MRT-LBM and code. In the simulation, a $100 \times 300$ mesh grid is used, a symmetric electrolyte solution is considered ($z_+ = -z_- = z = 1$). The other physical parameters are: the dielectric constant of the solution $\varepsilon_r \varepsilon_0 = 7.79 \times 10^{-10} C^2/Jm$, the thermodynamic temperature $T = 273K$, the density $\rho = 1.0 \times 10^3 kg/m^3$, $\nu_0 = 1.789 \times 10^{-6} m^2/s$, $k_B = 1.38 \times 10^{-23} J/K$, the surface zeta potential of $\zeta = -100$mV and the externally applied electric field intensity $E = 500V/m$. The Debye length, $\lambda_D$, which is used to describe the characteristic thickness of the electric double layer (EDL), is defined as follows,

$$\lambda_D = \sqrt{\frac{\varepsilon_r \varepsilon_0 k_B T}{2 N_A c_0 e^2 z^2}}, \tag{4.1}$$

where $c_0$ is the bulk ionic concentration. To be consistent with previous work [40], the bulk ionic concentrations $c_0 = 10^{-7}$mol/l and $c_0 = 10^{-4}$mol/l are both considered.

Fig. 3 presents the numerical results (symbols) of the normalized streamwise velocity profile across the channel compared to the existing data (solid lines) [40] for $c_0 = 10^{-7}$mol/l and $c_0 = 10^{-4}$mol/l, respectively. The value of $\lambda_D/H$ for $c_0 = 10^{-7}$mol/l is 0.029, while for $c_0 = 10^{-4}$mol/l, $\lambda_D/H = 1.01$. It can be clearly seen that the LBM results have a good agreement with the previous work over the range of $n$ parameter values. The velocity profiles for Newtonian fluid of $n = 1$ is parabolic, which resembles a typical pressure-driven flow. However, for the shear thinning ($n = 0.5$) flows, we can see a general flattening of the velocity flows. Whereas, for the case of shear thickening ($n > 1$) flows, the velocity profiles for $n = 2.0$ and $3.0$ present greater curvature and sharp-like
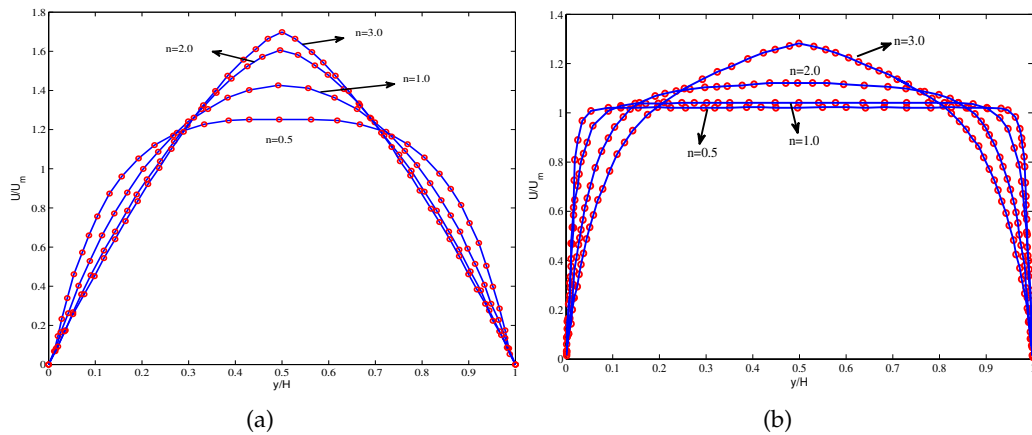
(a)                                    (b)

Figure 3: Comparison between the numerical results and the existing data: (a) $c_0 = 10^{-7}$mol/l; (b) $c_0 = 10^{-4}$mol/l.
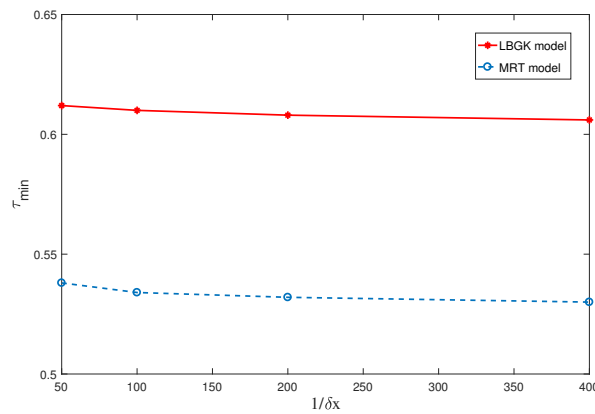


Figure 4: Minimum value of $\tau_{n_k}$ by MRT model and LBGK model.

around the center peak velocity. These numerical predictions are also consistent with the results in [40].

To illustrate the stability of the proposed MRT model, the minimum value of the relaxation time $\tau_{\min}$ in the LBM for Nernst-Planck equation is computed by the LBGK model and MRT model, respectively. From Fig. 4, we can see that the $\tau_{\min}$ computed by the LBGK model is around 0.61, while for the MRT model, the value of $\tau_{\min}$ is around 0.53. This illustrates that in the numerical study of electrokinetic flow of power-law fluids, the MRT model is more stable than the LBGK model. All the computations are carried out on the Intel (R) Core (TM) i7-3820 CPU with 8 cores of 3.60 GHz. In addition, the collision part of MRT and SRT models are both performed on Graphics Processing Unit (GPU) of Tesla K20c using NVIDIAs CUDA 5.0. To compare the numerical efficiency of MRT
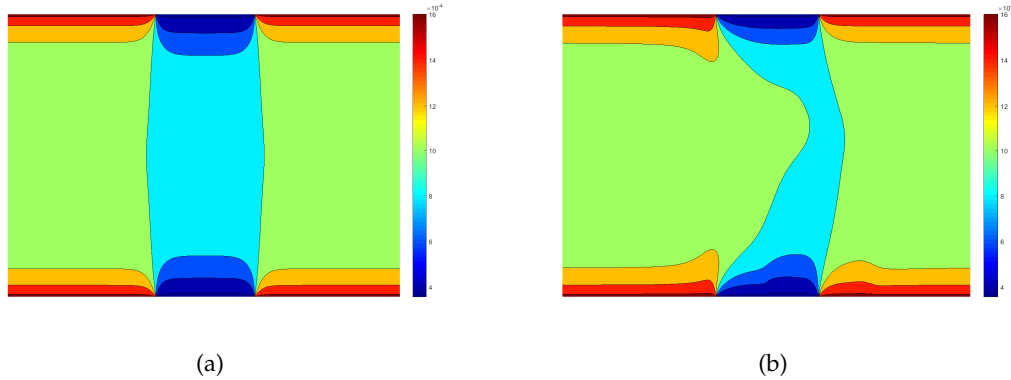
(a)                                                            (b)

Figure 5: Comparison of ionic distribution of PB model and N-P model: (a) PB model; (b) N-P model.

and SRT models, the GPU times ($T_{GPU}$) for these two models is measured. After 10000 iterations, the $T_{GPU}$ of MRT model is about 69.82s, while for SRT model, $T_{GPU} = 61.69$s.

In addition, to present the difference between the N-P model and PB model in describing the ionic distribution in micro-channel with non-uniform surface potential, a symmetrically arranged structure with $\psi_p = -\zeta$ is considered. Numerical comparison of these two models are depicted in Fig. 5. As we can see, the ionic distribution of PB model is symmetric and not affected by the flow field, while for the N-P model (see Fig. 5(b)), the ionic distribution is distorted due to the interaction of the flow field and ionic concentration field. These results demonstrate that the N-P model is more applicable to describe the ionic distribution of EOF with nonuniform surface potential.

## 4.2   Effects of non-uniform surface potential and power-law index on the mixing efficiency

In this section, we are focusing on how the heterogeneous surface charge and power-law index influence the mixing efficiency. Our simulation results are presented here for a symmetric electrolyte with an ionic molar concentration of $10^{-4}$mol/l ($\lambda_D/H = 0.029$). While the other parameters are same as the last section and a $100 \times 1000$ mesh grid is used. In addition, the modified Reynolds number ($Re$) for the power-law fluid can be written as $Re = u_{av}^{(2-n)} H^n / \nu_0$, where $u_{av}$ is the average velocity. For example, when the fluid is Newtonian ($n = 1$), Reynolds number is equal to 0.03. While for the shear-thinning fluid ($n = 0.8$), $Re = 0.038$, for the shear-thickening fluid ($n = 1.2$), $Re = 0.023$. The other dimensionless parameter $Pe$ and $StPe$ are less than order $10^2$ and $10^4$, respectively.

Next, we choose the power-law index varies in the range of 0.6-1.6 and change the non-uniform surface potential $\psi_p$ from 0 to 25mV with a 5mV increment, whereas the surface potential remains at a constant value of -25mV. Without loss of generality, we present the flow patterns of pow-law index $n = 1$ for symmetrically and asymmetrically arranged nonuniform surface potential in Fig. 6. As expected, a reverse flow occurs near
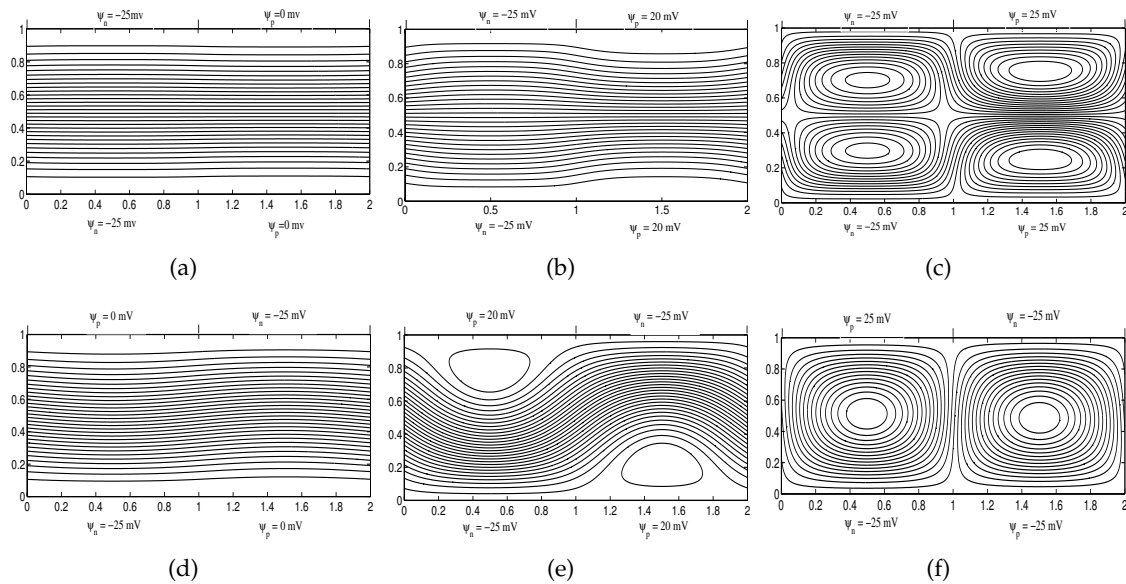
Figure 6: Flow patterns: (a) symmetric structure $\psi_p=0$mV, $\psi_n=-25$mV; (b) symmetric structure $\psi_p=20$mV, $\psi_n=-25$mV; (c) symmetric structure $\psi_p=25$mV, $\psi_n=-25$mV; (d) asymmetric structure $\psi_p=0$mV, $\psi_n=-25$mV; (e) asymmetric structure $\psi_p=20$mV, $\psi_n=-25$mV; (c) asymmetric structure $\psi_p=25$mV, $\psi_n=-25$mV.

the heterogeneous region with a positive surface potential. However, there is no vortex appeared for both symmetric and asymmetric structures when $\psi_p=0$mV. As $\psi_p$ increases to 20mV, the magnitude of the circulation also increases. We can clearly see the presence of flow disturbances in the heterogeneous regions in Figs. 6(b) and 6(e). Especially for the asymmetric structure, two eddies can be found in the vicinity of the heterogeneous patches. Furthermore, when $\psi_p$ continue to increase to 25mV, a larger recirculation region can be observed for the two types arrangement of patches in Figs. 6(c) and 6(f). It is also apparent that the flow patterns are quite different due to the rearrangement of the heterogeneous patches. From the above, we can see that the flow flied is effectively disturbed by the increased nonuniform surface potential $\psi_p$, which implies the higher mixing efficiency. But, it seems like the asymmetric structure of the heterogeneous patches are more helpful to enhance the mixing efficiency. In addition, the flow field patterns of shear thinning and shear thicken flows are similar to the case of $n=1$, so we did not present here.

Next, to explore the effects of power-law index and nonuniform surface potential on the mixing efficiency quantitatively, the mixing efficiency is measured at the outlet of microchannel. Fig. 7 shows the variation of the mixing index $\alpha$, which is defined in Section 2.3, with the power-law index and $\psi_p$. As we can see, for the two cases of arrangement of patches, the mixing efficiency increases with an increasing nonuniform surface potential. It also can be observed that the mixing efficiency of the asymmetric structure is slightly
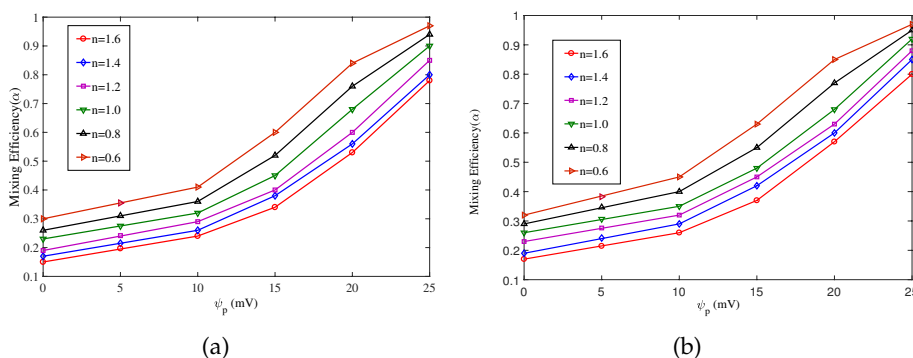
Figure 7: Mixing efficiency under different power-law index and non-uniform surface potential: (a) symmetric structure; (b) asymmetric structure.

higher than the symmetric case, which is coincidence with the flow patterns in Fig. 6. In addition, it is worth noting that as the increase of power-law index, the mixing efficiency decreased, which means the pseudoplastic fluids have a higher mixing efficiency than the dialatant fluids. Thus, in order to achieve a perfect mixing of dilatant fluids, there should be distributed more asymmetric charged patches.

## 4.3 Effects of non-uniform surface potential and power-law index on the volumetric flow rate

From the above section, we can see that EOF with heterogeneous surface potential appears to be an excellent alternative to enhance mixing efficiency, especially for the asymmetric distribution of the heterogeneous patches. However, as reported in [41], the nonuniform surface potential affects not only the flow field but also the flow rate for liquid transport. There should be a tradeoff between mixing and liquid transportation. To measure the liquid transport quantitatively, a dimensionless volumetric flow rate $Q/Q_{\max}$ at the outlet is introduced and

$$Q = \int_H u(x)Hdx,$$

where $H$ is the width of the microchannel, $u(x)$ is the velocity in the $x$ direction at outlet, $Q_{\max}$ is the flow rate of the same channel having a uniform surface potential of $\psi_n = -25$mV for power-law index $n=1$.

Fig. 8 shows the variation of normalized volumetric flow rate with power-law index and non-uniform surface potential for two types arrangement of heterogeneous patches. As we can see, the flow rate decreases with the increase of $\psi_p$ for both shear thinning and shear thickening flows, which illustrates that excellent mixing lead to a poor transport of electroosmotic flow. It also can be observed that the symmetric and asymmetric arrangement of nonuniform surface potential have the same flow rate with the different values of $\psi_p$, which means the electroosmotic flow rate is independent on the arrangement of
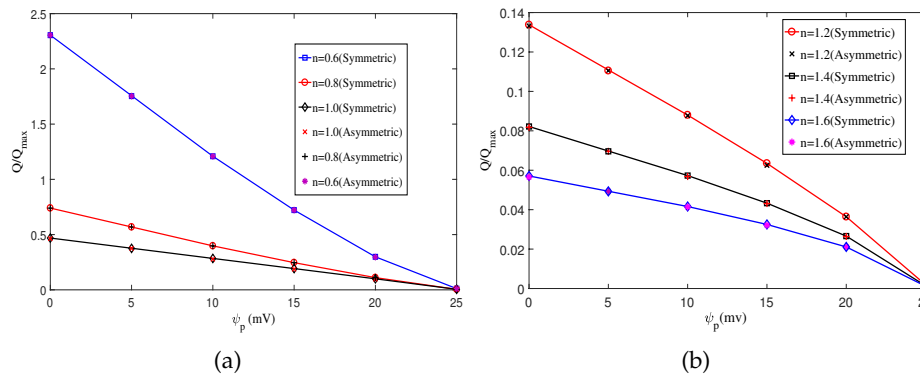
Figure 8: Variation of normalized volumetric flow rate with power-law index and non-uniform surface potential: (a) Shear thinning flows; (b) Shear thickening flows.

heterogeneous patches. Furthermore, through comparing with Fig. 8(a) and Fig. 8(b), we can see that $Q/Q_{\max}$ for shear thinning flow is larger than the thicken flow, whereas for the case of $\psi_p = 25\mathrm{mV}$, the $Q/Q_{\max}$ for shear thinning and shear thickening flows are both close to zero.

# 5    Conclusions

In this work, we proposed a coupled MRT-LB framework for the dynamic model of electrokinetic driven flow of non-Newtonian fluid. In the dynamic model, a more accurate N-P model other than PB model is used to describe the ionic distribution in the EDL. In what follows, the micromixing of non-Newtonian fluids with power-law behavior in microchannels with heterogeneous surface potential has been numerically studied by the proposed MRT-LBM. The effects of the arrangement of nonuniform surface potentials and the power-law index on the mixing performance and the volumetric flow rate were systematically examined. The numerical results indicate that the mixing efficiency of the asymmetric distribution of non-uniform surface potential is higher than the symmetric one for both shear-thinning and shear thicken flows. It also has been shown that the mixing performance of non-Newtonian fluids can be improved by increasing the non-uniform surface potential, whereas the mixing efficiency is decreased with the increases of power-law index. In addition, the flow rate decreases with the increase of non-uniform surface potential for both shear thinning and shear thickening flows, which implies that excellent mixing lead to a poor transport of EOF and there should be a tradeoff between the mixing and liquid transport in electrokinetic microfluidics.

# Acknowledgements

# References

[1] M. GADEL HAK, The MEMS Handbook, CRC Press, 2002.

[2] H. A. STONE, A. D. STROOCK AND A. AJDARI, *Engineering flows in small devices: microfluidics toward a labon-a-chip,* Annu. Rev. Fluid Mech., 36 (2004), pp. 381–411.

[3] Z. CAI, R. LI AND Z. QIAO, *NRxx simulation of microflows with Shakhov model,* SIAM J. Sci. Comput., 34 (2012), pp. A339–A369.

[4] J. M. LEHN, *Supramolecular chemistry-scope and perspectives molecules, supermolecules and molecular devices*, Angew. Chem. Int. Ed., 27 (1988), pp. 89–112.

[5] A. AJDARI, *Electro-Osmosis on inhomogeneously charged surfaces,* Phys. Rev. Lett., 75 (1995), pp. 755–758.

[6] A. AJDARI, *Generation of transverse fluid currents and forces by an electric field: Electro-osmosis on charge-modulated and undulated surfaces,* Phys. Rev. E, 53 (1996), 4996.

[7] Z. QIAO, Z. LI AND T. TANG, *Efficient numerical methods for the 2D nonlinear Poisson-Boltzmann equation modeling charged spheres,* J. Comput. Math., 24 (2006), pp. 252–264.

[8] Z. LI, C. PAO AND Z. QIAO, *A finite difference method and analysis for 2D nonlinear Poisson-Boltzmann equations,* J. Sci. Comput., 30 (2007), pp. 61–81.

[9] E. Y. K. NG AND S. T. TAN, *Study of EDL effect on 3-D developing flow in microchannel with Poisson-Boltzmann and Nernst-Planck models,* J. Numer. Meth. Eng., 71 (2007), pp. 818–836.

[10] H. M. PARK, J. S. LEE AND T. W. KIM, *Comparison of the Nernst-Planck model and the Poisson-Boltzmann model for electroosmotic flows in microchannels,* J. Colloid Interf. Sci., 315 (2007), pp. 731–739.

[11] Y. S. CHOI AND S. J. KIM, *Electrokinetic flow-induced currents in silica nanofluidic channels,* J. Collid Interf. Sci., 333 (2009), pp. 672–678.

[12] M. WANG AND Q. KANG, *Modeling electrokinetic flows in microchannels using coupled lattice Boltzmann methods,* J. Comput. Phys., 229 (2010), pp. 728–744.

[13] S. CHEN AND G. DOOLEN, *Lattice Boltzmann method for fluid flows,* Annu. Rev. Fluid Mech. 30 (1998), pp. 329–364.

[14] Z. GUO, AND C. SHU, Lattice Boltzmann Method and Its Applications in Engineering, World Scientific, 2013.

[15] S. SUCCI, The Lattice Boltzmann Equation for Fluid Dynamics and Beyond, Oxford University Press, 2001.

[16] B. CHOPARD, J. L. FALCONE AND J. LATT, *The lattice Boltzmann advection-diffusion model revisited,* Eur o. Phys. J. Spec. Top., 171 (2009), pp. 2450–249.

[17] Z. CHAI, AND T. S. ZHAO, *Lattice Boltzmann model for the convection-diffusion equation,* Phys. Rev. E, 87 (2013), 063309.

[18] B. SHI AND Z. GUO, *Lattice Boltzmann model for nonlinear convection-diffusion equations,* Phys. Rev. E, 79 (2009), 016701.

[19] Z. CHAI, B. C. SHI AND Z. L. GUO, *A multiple-relaxation-time lattice Boltzmann model for general nonlinear anisotropic convection-diffusion equations,* J. Sci. Comput., 69 (2016), pp. 355–390.

[20] C. S. HUANG, B. C. SHI, N. Z. HE AND Z. H. CHAI, *Implementation of multi-GPU based lattice Boltzmann method for flow through porous media*, Adv. Appl. Math. Mech., 7 (2015), pp. 1–12.

[21] X. HE AND N. LI, *Lattice Boltzmann simulation of electrochemical systems*, Comput. Phys. Commun., 129 (2000), pp. 158–166.

[22] X. G. YANG, B. C. SHI, Z. H. CHAI AND Z. L. GUO, *A coupled lattice Boltzmann method to solve Nernst-Planck model for simulating electro-osmotic flows*, J. Sci. Comput., 61 (2014), pp. 222–238.

[23] M. HADIGOL, R. NOSRATI, A. NOURBAKHSH AND M. RAISEE, *Numerical study of electro-osmotic micromixing of non-Newtonian fluids*, J. Non-Newtonian Fluid Mech., 166 (2011), pp. 965–971.

[24] C. ZHAO, E. ZHOLKOVSKIJ, J. H. MASLIYAH AND C. YANG, *Analysis of electroosmotic flow of power-law fluids in a slit microchannel*, J. Colloid Interface Sci., 326 (2008), pp. 503–510.

[25] M. SHAMSHIRI, R. KHAZAELI, M. ASHRAFIZAADEH AND S. MORTAZAVI, *Electroviscous and thermal effects on non-Newtonian liquid flows through microchannels*, J. Non-Newtonian Fluid Mech., 173-174 (2012), pp. 1–12.

[26] C. C. CHO, C. L. CHEN, AND C. K. CHEN, *Mixing of non-Newtonian fluids in wavy serpentine microchannel using electrokinetically driven flow*, Electrophoresis, 33 (2012), pp. 743–750.

[27] R. B. M. SCHASFOORT, S. SCHLAUTMANN, J. HENDRIKSE, AND A. VAN DER BERG, *Field-effect flow control for microfabricated fluidic networks*, Science, 286 (1999), 942.

[28] Z. H. CHAI, B. C. SHI, Z. L. GUO AND F. M. RUO, *Multiple-relaxation-time lattice Boltzmann model for generalized Newtonian fluid flows*, J. Non-Newton. Fluid, 166 (2011), pp. 332–342.

[29] Z. H. CHAI AND T. S. ZHAO, *Effect of the forcing term in the multiple-relaxation-time lattice Boltzmann equation on the shear stress or the strain rate tensor*, Phys. Rev. E, 86 (2012), 016705.

[30] P. NEOFYTOU, *A 3rd order upwind finite volume method for generalised Newtonian fluid flows*, Adv. Eng. Software, 36 (2005), pp. 664–680.

[31] M. R. WANG AND Q. J. KANG, *Modeling electrokinetic flows in microchannels using coupled lattice Boltzmann methods*, J. Comput. Phys., 229 (2010), pp. 728–744.

[32] P. LALLEMAND AND L.-S. LUO, *Theory of the lattice boltzmann method: dispersion, dissipation, isotropy, galilean invariance and stability*, Phys. Rev. E, 61 (2000), pp. 6546–6562.

[33] X. HE AND L. S. LUO, *Lattice Boltzmann model for the incompressible Navier-Stokes equation*, J. Stat. Phys., 88 (1997), pp. 927–944.

[34] Z. L. GUO Z, C. G. ZHENG AND B. C. SHI, *Discrete lattice effects on the forcing term in the lattice Boltzmann method*, Phys. Rev. E, 65 (2002), 046308.

[35] D. CONTRINOA, P. LALLEMAND, P. ASINARI AND L. S. LUO, *Lattice-Boltzmann simulations of the thermally driven 2D square cavity at high Rayleigh numbers*, J. Comput. Phys., 275 (2014), pp. 257–272.

[36] Z. H. CHAI AND T. S. ZHAO, *Nonequilibrium scheme for computing the flux of the convection-diffusion equation in the framework of the lattice Boltzmann method*, Phys. Rev. E, 90, (2014), 013305.

[37] X. G. YANG, B. C. SHI AND Z. H. CHAI, *Generalized modification in the lattice Bhatnagar-Gross-Krook model for incompressible Navier-Stokes equations and convection-diffusion equations*, Phys. Rev. E, 90, (2014), 013309.

[38] Q. LI AND K. H. LUO, *Effect of the forcing term in the pseudopotential lattice Boltzmann modeling of thermal flows*, Phys. Rev. E, 89, (2014), 053022.

[39] Z. H. CHAI AND B. C. SHI, *A novel lattice Boltzmann model for the Poisson equation*, Appl. Math. Model., 32 (2008), pp. 2050–2058.

[40] G. H. TANG, X. F. LI, Y. L. HE AND W. Q. TAO, *Electroosmotic flow of non-Newtonian fluid in*

*microchannels,* J. Non-Newtonian Fluid Mech. 157 (2009), pp. 133–137.

[41]  F. Z. TIAN, B. M. LI AND D. Y. KWOK, *Tradeoff between mixing and transport for electroosmotic flow in heterogeneous microchannels with nonuniform surface potentials,* Langmuir, 21 (2005), pp. 1126–1131.